6-2017

The magnetic, electrical and structural properties of copper-permalloy alloys

Makram A. Qader
Arizona State University

A. Vishina
Kings College London

Lei Yu
Arizona State University

Cougar Garcia
Arizona State University

Rakesh K. Singh
Kurukshetra University

See next page for additional authors

Authors
Makram A. Qader, A. Vishina, Lei Yu, Cougar Garcia, Rakesh K. Singh, Nicholas D. Rizzo, Mengchu Huang, Ralph Chamberlin, Kirill Belashchenko, Mark van Schilfgaarde, and N. Newman

Published in *Journal of Magnetism and Magnetic Materials* 442 (2017), pp 45–52.
doi 10.1016/j.jmmm.2017.06.081

Submitted 23 February 2017; revised 17 May 2017;
accepted 14 June 2017; published 17 June 2017.

The Magnetic, Electrical and Structural Properties of Copper-Permalloy Alloys

Makram A. Qader,[1] Alena Vishina,[2] Lei Yu,[1] Cougar Garcia,[3] R. K. Singh,[3] N. D. Rizzo,[4] Mengchu Huang,[3] Ralph Chamberlin,[5] K. D. Belashchenko,[6] Mark van Schilfgaarde,[2] and N. Newman [1,3]

1 Electrical Engineering Department, Arizona State University, Tempe, AZ 85287-9309, USA
2 King's College London, London, England WC2R 2LS, United Kingdom
3 Materials Program, SEMTE, Arizona State University, Tempe, AZ 85287-6106, USA
4 Northrop Grumman Corporation, Linthicum, MD 21090, USA
5 Department of Physics, Arizona State University, Tempe, AZ 85287-1504, USA
6 Department of Physics and Astronomy and Nebraska Center for Materials and Nanoscience, University of Nebraska–Lincoln, Lincoln, NE 68588, USA

Corresponding author — N. Newman, Materials Science Program, Arizona State University, Tempe, AZ 85287-6106, USA; *email* Nathan.Newman@asu.edu

Abstract

Copper-permalloy [$Cu_{1-x}(Ni_{80}Fe_{20})_x$] alloy films were deposited by co-sputtering and their chemical, structural, magnetic, and electrical properties were characterized. These films are found to have favorable weak ferromagnetic properties for low temperature magnetoelectronic applications. Our results show that by varying the composition, the saturation magnetization (M_s) can be tuned from 700 emu/cm^3 to 0 and the Curie temperature (T_c), can be adjusted from 900 K to 0 K. The M_s and T_c are found to scale linearly between x = 25% and 100%. Electronic structure calculations are used to provide a strong fundamental understanding of the mechanisms responsible for establishing the observed electrical and magnetic properties. The theoretical results also show that the introduction of Cu into the permalloy lattice results in very strong spin scattering in the minority spin channel, with only moderate interactions in the majority channel.

1. Introduction

The use of doping and alloying of magnetic materials can be used to engineer the properties of magnets for practical applications. Beginning in the 1930s, many advances were made in systematic studies of a wide range of dopants and alloying agents, led by Elmen, Bozarth and others in the Bell Labs group [1,2]. Their quest led to metallic magnets with high permeabilities and low a.c. loss for transformers and loading coils, large remanent magnetizations for permanent magnets, and oxide ferrites and garnets for high frequency applications. In all these cases, the materials are comprised largely of "magnetic" elements, e.g. Co, Ni, Fe, Cr, and Mn, and are classified as "strong" since they exhibit characteristically large saturation magnetization values (or equivalently high permeabilities) at room temperature. The use of magnets at low temperatures for practical applications is limited to date, and when they are used, strong magnets are almost always chosen because of their high saturation magnetization (M_s).

The exploration of dilute levels of the magnetic elements in non-magnetic hosts has not been extensively explored for practical applications because magnetic ordering is only observed at low temperatures and the magnetism is weak. Most previous work on dilute magnetic systems has been done primarily by the academic community in areas such as spin glasses [3]. The magnetic behavior of dilute magnets can be understood using a combination of RKKY theory and percolation models. [4–6]

Besides the questions associated with the fundamental issues and properties of dilute magnets, there has been a growing need for weak magnets with low saturation magnetization and possibly reduced Curie temperature for some microelectronic applications. To reduce the switching fields of spin-toggle MRAM, the use of weaker magnets operating at lower temperatures is a viable alternative. Since the thermal stability barrier of a single-domain bit in the Stoner-Wohlfarth model scales as $M_s^2 \Delta t^2 \propto k_B T$ [7,8], (Δt is the layer thickness, and T is the temperature associated with the thermal stability criterion used to evaluate bit retention), and the minimum write current that generates the switching field scales as $M_s \Delta t$, a reduction from 300 to 4 K would allow a factor of $(300/4)^{1/2} \approx 8.6$ in the write field and current.

In order to increase the density of MRAM devices, there is strong interest in developing practical spin-torque MRAM device technology. For these spin-torque MRAM devices, the write current (I_c) scales

roughly proportional to M_s^2 [7]. Such a reduction is important to reducing the power consumption during low temperature operation. It could also help to minimize the current-induced damage to the tunnel barriers that can limit the lifetime of today's room temperature spin torque MRAM devices.

Another microelectronic application of interest is the development of a fast, dense, low-power cryogenic memory that uses Cooper pair transport though ferromagnetic free and fixed layers clad by superconducting electrodes [9–11]. Since the read process detects the zero-voltage superconducting current magnitude, the act of reading a bit consumes an inconsequential amount of energy. Thus, the switching energy of the free layer determines the power requirements of the memory and is identical to the write cycle of MRAM. It can be reduced using a low M_s free layer [9–11].

In the work described here we show that by diluting magnetic elements with non-magnetic hosts, the properties including the saturation magnetization and Curie temperature can be tuned down to desired small values. We specifically study copper-permalloy ($Cu_{1-x}(Ni_{80}Fe_{20})_x$) alloys in the magnetically dilute limit, where M_s can be tuned from 700 emu/cm^3 to 0 and the T_c can be adjusted from 900 K to 0 K by varying the alloy composition. Studies of the structural and chemical properties of this alloy system have determined that the Cu-permalloy system is miscible over a wide range of compositions [12]. To our knowledge, the magnetic and electronic properties have not been explored extensively, particularly in the dilute limit of permalloy content.

2. Methods

Cu-permalloy films used for this study were deposited at room temperature onto oxidized Si (100) wafers using co-sputtering in an unbaked UHV chamber with a base pressure of ~2×10^{-8} Torr. 5 cm U.S. Inc. and 2.5 cm Kurt Lesker Torus™ magnetron sputter sources were used with 99.95% pure $Ni_{81}Fe_{19}$ (81% Ni, and 19% Fe) and 99.99% Cu targets, respectively. The $Ni_{81}Fe_{19}$ source sputters head-on to the substrate and the Cu source was mounted at a 45° angle. The films were sputtered under an Ar pressure of 3 mTorr and an Ar flow rate of 70 sccm. The power of the Cu and $Ni_{81}Fe_{19}$ sources were varied from 2 to 200W to controllably adjust the Cu content of the deposited films.

These conditions and this target composition are known to produce $Ni_{80}Fe_{20}$ permalloy films. Using this technique, the entire range of alloy compositions $Cu_{1-x}(Ni_{80}Fe_{20})_x$ ($0 < x \leq 1$) was achieved. Rutherford backscattered spectrometry (RBS) was used to infer Cu content and the thickness of the thin films. The density of thin films used in the RBS analysis was obtained from X-ray reflectivity (XRR) measurements. Since the involved elements (Cu, Ni, Fe) have close atomic weights, reducing the accuracy of the RBS analysis, the composition was further verified by particle induced X-ray emission spectroscopy (PIXE) for a number of films. We found the composition variation, Δt, across a 1 cm × 1 cm area was less than 5%.

The magnetic properties, temperature-dependent magnetization, and magnetization versus applied field (M-H) isotherm curves of the films were characterized using a vibrating sample magnetometer (VSM) from 2 to 1000 K (Quantum Design, Model PPMS with oven option). Only pure permalloy samples were measured at elevated temperatures with the oven option. The temperature dependent electrical resistivities of the films were measured using an inline 4-point dipping probe inserted into a liquid He Dewar. The surface quality and roughness of the thin films were obtained from topography measurements using a commercial atomic force microscope (AFM) (Veeco, Model Dimension 300).

We have carried out electronic structure calculations of Cu_y-$Ni_{1-x-y}Fe_x$ alloys, within the Local-Density Approximation (LDA), using the tight-binding Linear Muffin Tin Orbital (LMTO) basis and Atomic Sphere's Approximation (ASA) [13]. LMTO is an augmented wave method where smooth envelope functions are augmented by numerical solutions of the Schrodinger equation inside spheres centered around their nuclei. It differs from the Linearized Augmented Plane Wave (LAPW) method in that the smooth envelope functions are Hankel functions, rather than plane waves. The ASA consists of the following approximations: (1) It overlaps augmentation spheres so that their volume fills the entire unit cell. The interstitial contribution to the Hamiltonian is omitted. This approximation is quite reasonable in well packed systems of interest here. (2) It replaces the true potential inside the spheres with a spherical average, also a reasonable approximation for close packed systems. To treat disorder, a Green's function approach was used in the Coherent Potential Approximation (CPA). We adopt an approach similar to that of Turek et al. [14], except that we combine CPA with third order potential functions [15]. In the CPA,

broadening of a band by alloy scattering is given by the imaginary part of the self-energy at the quasiparticle peak. The lattice constant used is 3.57 Å taken from [16] reduced by 0.2%; the valence basis consisted of s-, p-, and d-orbitals.

3. Experimental results

RMS roughness and thickness of a few $Cu_{1-x}(Ni_{80}Fe_{20})_x$ compositions are summarized in **Table 1**. The 1–2 nm rms surface roughness values indicate that the topography of the film is relatively smooth for all of the listed films and should be adequate for thin-film magnetoelectronic applications.

Fig. 1 shows the typical M-H behavior of co-sputtered $Cu_{1-x}(Ni_{80}Fe_{20})_x$ alloy films at room temperature (RT) and 4.2 K. This particular sample has 50% Permalloy content and measured Curie temperature of 380 K.

Table 1. RMS roughness of a few $Cu_{1-x}(Ni_{80}Fe_{20})_x$ films, as measured by AFM.

Permalloy content (%)	Thickness (nm)	RMS roughness (nm)
60	72	1.4
30	83	1
12	115	1.8

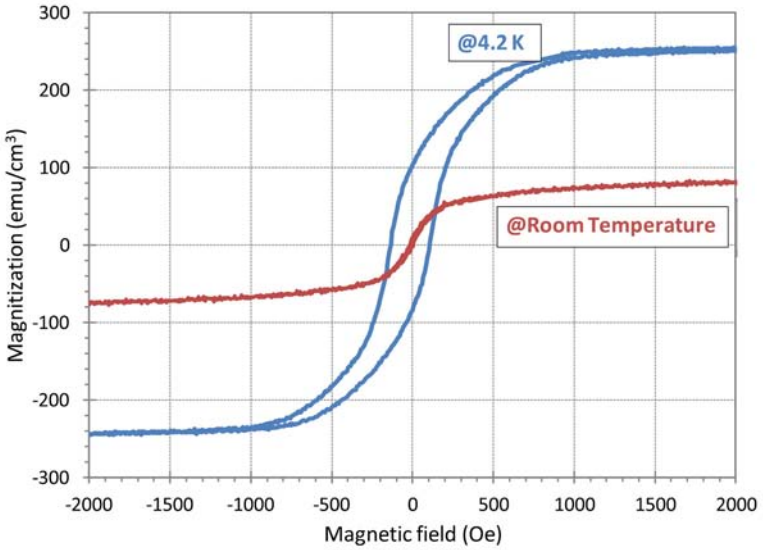

Fig. 1. Typical M-H behavior of co-sputtered Cu-Permalloy alloy. This particular sample has 50% Permalloy content and a Curie temperature of 380 K.

As a result, at room temperature when T = 300 K is near T_{curie}, the data shows near-zero coercivity H_c and magnetic remanence M_r, as well as a lack of complete magnetic moment saturation at high fields. All of which are characteristic features of superparamagnetism. In contrast at T = 4.2 K, the H_c, and M_r are finite, and the magnetic moment saturates completely, consistent with a strongly ferromagnetic film.

Temperature-dependent saturation magnetizations of representative $Cu_{1-x}(Ni_{80}Fe_{20})_x$ alloys are shown in **Fig. 2**. The data were measured under an applied field of 2500 Oe, large enough to reach saturation at all temperatures for all samples in this study. For x = 0.75, the temperature-dependent saturation magnetization can be fit to a Brillouin function [17], which is typical of strong ferromagnetic materials like permalloy. In this case, it is possible to extract the Curie temperature values from fitting the M_s-T curves. However, for x = 0.35 and x = 0.25 the M_s-T data deviate from the Brillouin function, likely due to the influence of the relatively large applied magnetic field compared to the relatively weak internal field of the material. Other materials with similarly small exchange energies and saturation magnetic fields behave similarly.

In order to avoid the large inaccuracies in such an analysis for weak magnets, we used Arrott analysis [18] to determine the Curie temperatures in this study. As illustrated in **Fig. 3**, low field M_3 (where M is

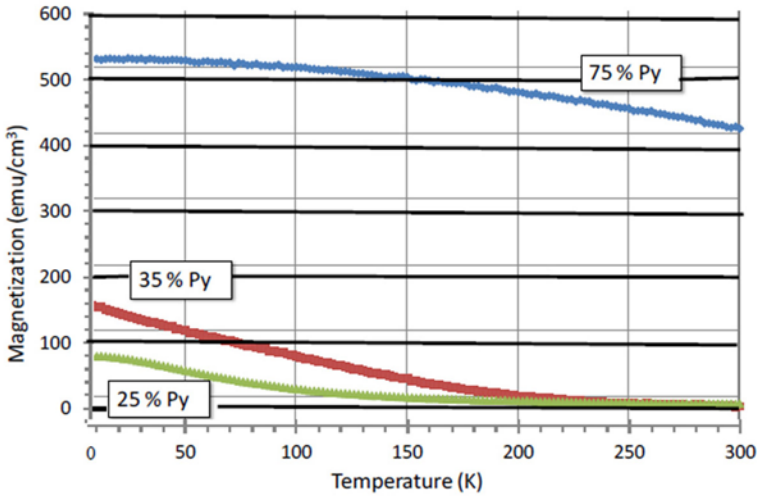

Fig. 2. Temperature-dependent magnetization of Cu-permalloy alloy measured at 2500 Oe. The magnetization was adjusted to zero to offset a small diamagnetic component resulting from the sample holder, and substrate.

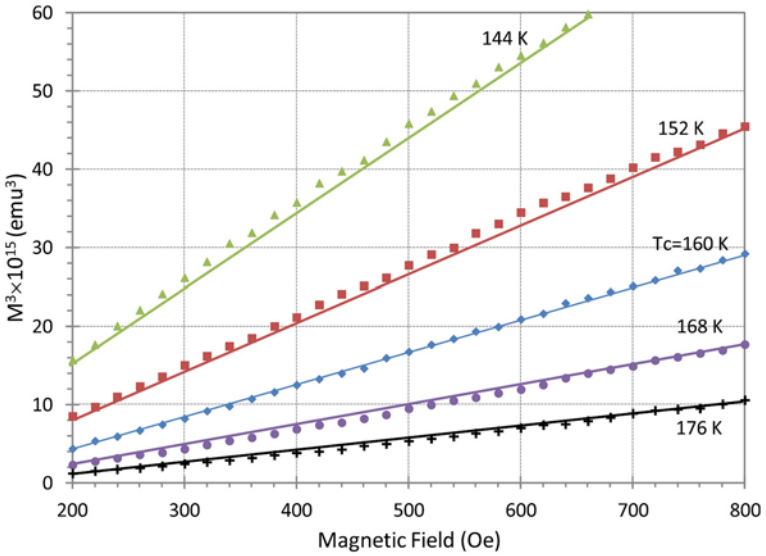

Fig. 3. Arrott analysis [13] was used to determine the Curie temperature (T_c) of $Cu_{1-x}(Ni_{80}Fe_{20})_x$ alloys. For temperatures above T_c, the shape of M^3 vs. H is concave up, and for temperatures below T_c, the shape of M^3 vs. H is concave down. At T_c, M^3 vs. H is linear. The data plotted here came from a sample that contains 35% Permalloy.

the magnetization) vs H curves at various temperatures were plotted. For temperature above T_c, the shape of M_3 vs. H is concave up, and for temperatures below T_c, the shape of M_3 vs. H is concave down. At T_c, M_3 vs. H is linear. As shown in **Fig. 3**, using this method we can determine T_c within a few degrees.

Fig. 4 summarizes the Curie temperature, saturation magnetization at 4.2 K, and coercive field (H_c) at 4.2 K as a function of permalloy content of co-sputtered $Cu_{1-x}(Ni_{80}Fe_{20})_x$ films. For the films studied, H_c is in the range of 120–150 Oe. In these types of alloys H_c is largely determined by domain wall motion and pinning which is extrinsic and influenced primarily by defects, such as grain boundaries and dislocations, structural relaxation effects, chemical clustering, thickness variation/surface irregularities, as well as exchange interaction or local anisotropy fluctuations [19]. These effects are independent of temperature and lead to an essentially flat H_c vs. T curve.

For permalloy content greater than 25%, T_c and M_s scale approximately linearly with Cu concentration (**Fig. 4**). For permalloy content below 25%, we were no longer able to extract reliable T_c values from Arrott analysis due to the small magnetization and significant noise.

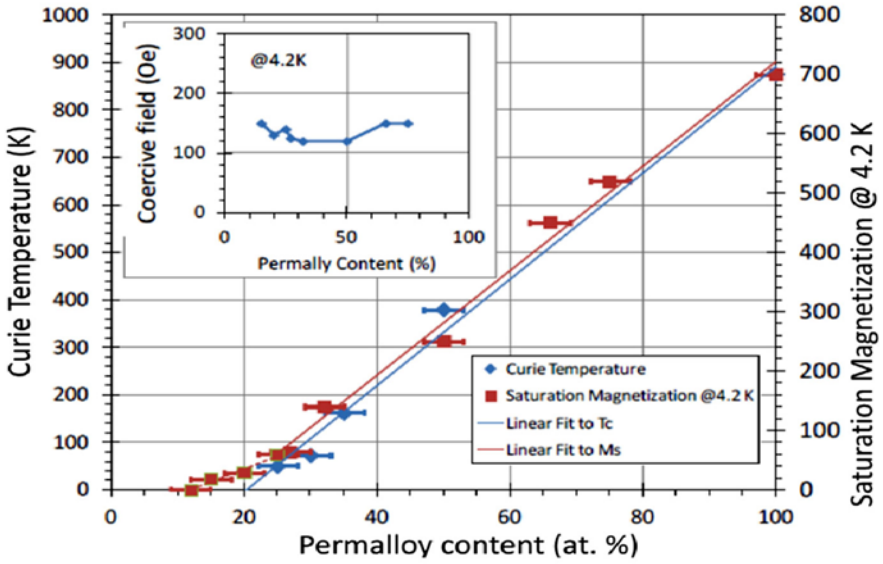

Fig. 4. Curie temperature (T_c), saturation magnetization (M_s) at 4.2 K, and coercive field (Hc) dependencies on Permalloy content of co-sputtered $Cu_{1-x}(Ni_{80}Fe_{20})_x$ films.

Between 12% and 25% Permalloy content, M_s values scale with a reduced slope as shown in **Fig. 4**.

Fig. 5(top) shows the magnetization measured in 5 kOe applied field as a function of temperature for two dilute permalloy alloys $Cu_{70}(Ni_{80}Fe_{20})_{30}$ and $Cu_{85}(Ni_{80}Fe_{20})_{15}$. **Fig. 5**(bottom) shows the magnetization versus applied field graphs (M-H loops) measured on the same thin films. The M-H loops of the $Cu_{70}(Ni_{80}Fe_{20})_{30}$ sample show the characteristics of a ferromagnetic material: square hysteresis loops that have a large remanent magnetization M_r, and therefore large remanent squareness $Sq = M_r/M_s$, along with clear magnetic saturation in relatively small fields. The 100 K MH loop for the $Cu_{70}(Ni_{80}Fe_{20})_{30}$ shows a transition to characteristic properties of a superparamagnet: $H_c \approx 0$, $Sq \approx 0$, and an S-shaped loop without magnetic saturation even in field as high as 5 kOe. A transition to superparamagnetic properties at T = 100 K is consistent with the Curie temperature of this sample $T_c \approx 100$ K. In contrast, the M-H loops for the $Cu_{85}(Ni_{80}Fe_{20})_{15}$ exhibit the S-shape characteristic curves of a superparamagnet at all temperatures measured down to as low as T = 2 K: essentially closed loops with no H_c, small M_r, and squareness (M_s/M_r), and a lack of magnetic saturation even to high fields. S-shaped loops are generally consistent with the Langevin function used to describe the magnetization

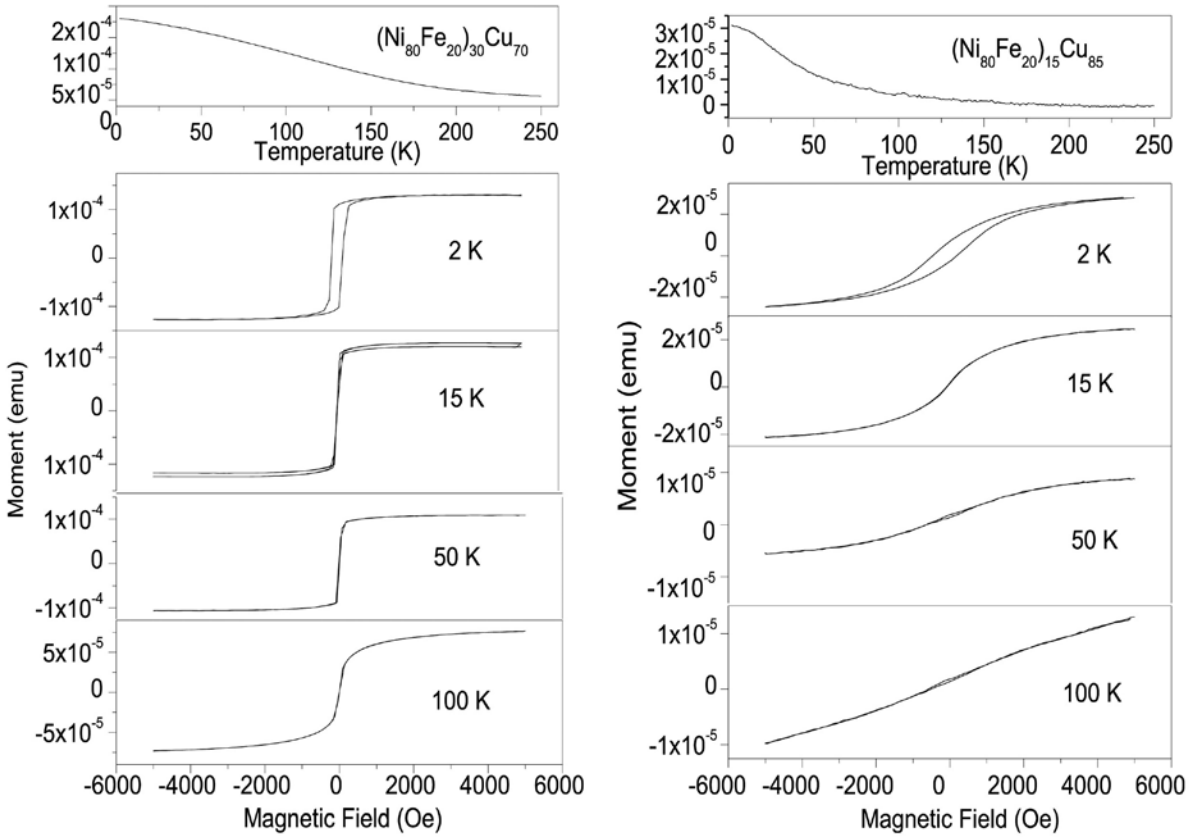

Fig. 5. (Top) Magnetization versus temperatures for 50 nm-thick $Cu_{70}(Ni_{80}Fe_{20})_{30}$ (left) and $Cu_{85}(Ni_{80}Fe_{20})_{15}$ (right) thin-films measured at a constant applied field of 5 kOe. (Bottom) The correspondence magnetization versus applied field for the same for 50 nm-thick $Cu_{70}(Ni_{80}Fe_{20})_{30}$ (left) and $Cu_{85}(Ni_{80}Fe_{20})_{15}$ (right) thin-films.

of superparamagnetic clusters [20]. The finite coercive field (H_c) at 2 K for the $Cu_{85}(Ni_{80}Fe_{20})_{15}$ film indicates that there is evidence of some ferromagnetic exchange coupling present in this inhomogeneous film. Based on these magnetic results, we conclude that the deviation from linearity observed in the M_s and T_c vs. NiFe content graphs (**Fig. 4**) occurring for NiFe content ≤25% is likely indicating a transition to an inhomogeneous NiFeCu mixture having regions of NiFe-rich material in a Cu-rich NiFeCu matrix. Such evidence for inhomogeneity seems reasonable given that Ni has complete solubility with Cu, while Fe has little to no solubility in Cu.

This linear dependence of T_c and M_s on permalloy content is similar to the behavior found by models with nearest-neighbor interactions as a function of dilution of magnetic entities with a non-magnetic

host [5]. Specifically, in the Ising model, binary (±) spins are randomly placed on a crystalline lattice. When the exchange interaction is restricted to nearest neighbors, a linear scaling of M_s and T_c is observed. Furthermore, this diluted Ising model predicts that ferromagnetic order disappears below a critical concentration of two magnetic nearest-neighbors per magnetic site, corresponding to a permalloy concentration of ~17% for the FCC lattice, in quantitative agreement with the critical concentration shown in **Fig. 4**. Although the agreement may be somewhat fortuitous, especially given the presence of spin fluctuations and other dynamical effects and the shape of the curvature as the critical concentration is approached, we believe that it gives insight into the physical nature of ferromagnetism in diluted magnetic materials. A more-realistic model would include spin fluctuations, as well as changes in the nearest-neighbor interactions when the number of neighbors is reduced, and the influence of next-nearest-neighbor interactions.

Despite the limitations mentioned above, simple models with fixed nearest-neighbor interactions are expected to be a reasonable approximation when the number of unpaired electron at each Ni and Fe atom remains relatively constant as Cu content increases. Chien et al. show that this is found for the case for Cu-Fe system [21], although it would be surprising for the Cu-Fe-Ni systems. Strong hybridization and shifts in the *d*-electron levels for such system occur, similar to those found in Au when alloyed with Ni to make white gold.

The observed linear relationship between Cu content, T_c and M_s is not found for other diluted Permalloy systems. For example, we found in Mo doped Permalloy made with similar method, at 14% Mo (86% $Ni_{80}Fe_{20}$) content, M_s dropped by ~15%, from ~700 to 600 emu/cm^3, while T_c has already dropped by almost 64% from ~900 to 325 K.

The $Cu_{1-x}(Ni_{80}Fe_{20})_x$ resistivity at room temperature and 4.2 K are summarized in **Fig. 6**. The presence of a peak at x = 50%, far away from the ferromagnetic transition at x = ~20%, and the relatively low resistivity compared to other metal-permalloy systems, suggests that alloy scattering, rather than magnetic scattering, is the dominant scattering mechanism in the majority channel of our films. In such alloy systems, the presence of one or more magnetic phases and disorders within the itinerant or localized spin systems will also cause scattering of conduction electrons.

The presence of ordering in the alloy could potentially also cause local minima in **Fig. 6**'s resistivity versus alloy curve, although we note

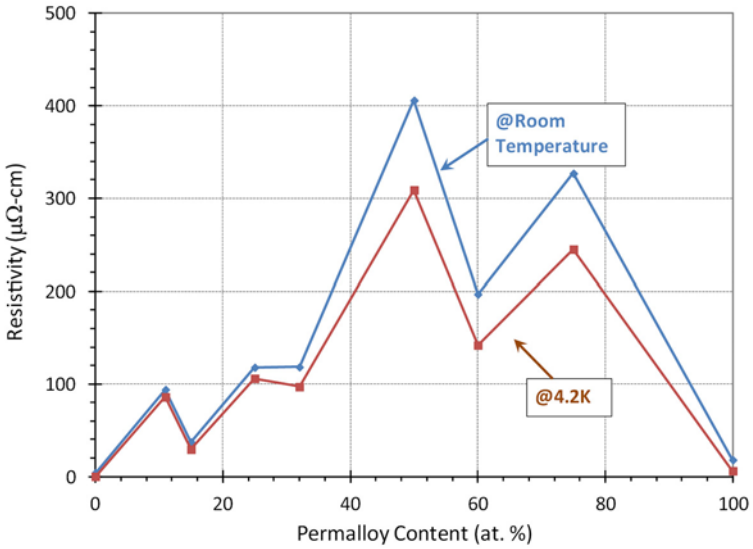

Fig. 6. The resistivity of Cu-Permalloy films at room temperature and 4.2 K for varying Permalloy content.

that the presence of their characteristic superlattice peaks were not observed in the X-ray diffraction pattern. In any case, we note that this behavior is very distinct from Cu-Ni alloys where the resistivity is found to peak at the concentration where the ferromagnetic transition occurs, at 45% Cu [22–24]. Some caution should be exercised before coming to strong conclusions about the electrical data for these $Cu_{1-x}(Ni_{80}Fe_{20})_x$ alloys since the phase diagram [12] does show a 2 phase region for 28% < x < 60%.

We have not observed evidence of a Kondo minimum in the temperature dependent resistivity of any $Cu_{1-x}(Ni_{80}Fe_{20})_x$ films that were measured.

4. Theoretical results

Electronic band structure calculations using the coherent potential approximation provide a fundamental basis for understanding the electrical and magnetic properties of the $Cu_{1-x}(Ni_{80}Fe_{20})_x$ alloys. Alloy scattering broadens out sharp quasiparticle levels and give them a width. Thus, the width of quasiparticle levels at the Fermi level are a direct measure of the alloy contribution to scattering of states there. In the CPA, broadening of a band by alloy scattering is given by the

imaginary part of the self-energy at the quasiparticle peak. Prior studies have shown energy band structure and some other characteristics of pure permalloy, for example [25–27], are in agreement with our results for the pure permalloy case.

For pure permalloy, we find scattering in the majority channel to be significantly smaller than in the minority channel. The weak scattering of the majority carriers explains the small resistivity of permalloy material. The presence of strong scattering of minority carriers at and near the Fermi level has important implications for spintronic devices, as well as the recently realized MRAM [8] and JMRAM devices [9–11].

The theoretical results in **Fig. 7** indicate that alloying with copper does not significantly change the general shape of the bands, but does introduce a moderate amount of alloy scattering for majority carriers and a large amount for minority carriers, particularly for large copper content. The enhanced scattering in the majority carrier channel can explain the higher resistivity of Cu-permalloy alloys than pure permalloy. We do note that scattering in copper-permalloy alloys is still lower than other metal-permalloy alloys [28].

One particular advantage of the LMTO method is that it generates from the potential a parameterized form of the scattering phase shift. These parameters (traditionally called "potential parameters"), define the Hamiltonian as shown below. There are two dominant parameters, C and Δ, which control most of the physics of the density-functional Hamiltonian. These parameters thus supply a great deal of physical insight, and are constructed in the following way (further details can be found in [15]).

We construct the "muffin-tin" orbitals that are continuous and differentiable in the form

$$\chi_{RL}(\varepsilon, \kappa, \mathbf{r}) = Y_L(\hat{\mathbf{r}}_R) \begin{cases} N_{Rl}(\varepsilon)\phi_{Rl}(\varepsilon, r_R) + P_{Rl}(\varepsilon)J_l(\kappa, r_R), & r_R < s \\ K_l(\kappa, r_R), & r_R > s \end{cases}$$

s is the nucleus radius, ε is the energy, κ is a "wave number," Y_L are the spherical harmonics, N_{Rl} and $P_{Rl}(\varepsilon)$ are coefficients fixed by requiring that the value and slope are continuous at $\mathbf{r}_R = \mathbf{r} - \mathbf{R}$. The P_{Rl} are called "potential functions" and play a central role in constructing eigenfunctions. Information about P can be encapsulated in a small number of

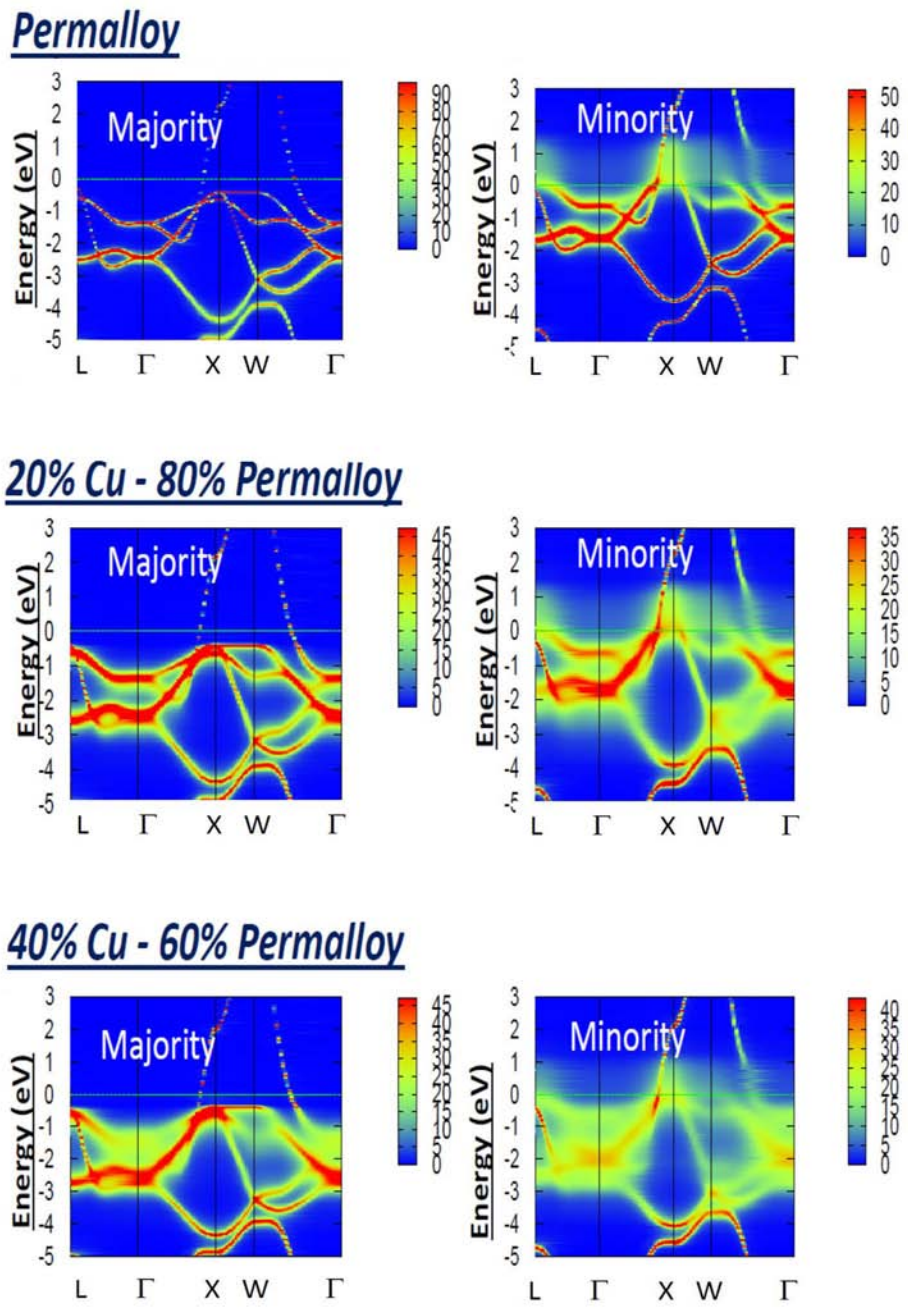

Fig. 7. Energy versus crystal momentum (k) band structure of the majority (left) and minority (right) bands. Broadening of the imaginary part of CPA self-energy (color bar, Ry) of majority (left) and minority (right) bands due to the alloy scattering. The width of the lines at the Fermi level (E = 0) is inversely proportional to the lifetimes of electron bands.

parameters: after linearizing the energy dependence of ϕ it can be parameterized to the second order in ε as

$$\tilde{P}(\varepsilon) = \left(\frac{\Delta}{\varepsilon - C} + \gamma \right)^{-1}$$

where γ, C and Δ are called "potential parameters" that parametrize P. There is one value of γ, C and Δ for each atom, orbital quantum number l, and spin. For alloy scattering, the crucial quantity will be how C varies between Cu, Fe and Ni in the d channel [28]. Any linear combination of χ_{RL} can be taken as a trial solution to Schrödinger's equation: $\Psi(\varepsilon, \kappa, r) = \sum_{RL} z_{RL} \chi_{RL} (\varepsilon, \kappa, r)$. χ_{RL} are Hankel functions that may be expanded about the origin as a linear combination of Bessel functions j_L

$$h_{RL}(\kappa, \mathbf{r}) = \sum_{M} S_{LM}(E, \mathbf{R}) j_L (\kappa, \mathbf{r})$$

The trial eigenfunction Ψ defined this way has a one-center expansion inside the sphere R

$$\phi_{RL}(\varepsilon, \mathbf{r})\, N_{RL}(\varepsilon) z_{RL}) + \left[J_{RL}(E, \mathbf{r}) P_{RL}(\varepsilon) z_{RL} - \sum_{L'} S_{RL',R'L}(E) J_{RL'}(E, \mathbf{r}) z_{RL} \right]$$

which satisfies Schrödinger's equation if the second and the third terms cancel. This leads to the "tail-cancelation" theorem [28]

$$\sum_{RL} \left[P_{RL}(\varepsilon) \partial_{R'L',RL} - S_{R'L',RL}(E) \right] z_{RL} = 0$$

ASA-tail cancelation reduces the problem to the form of the linear algebraic eigenvalue problem. A non-trivial solution of this problem requires the determinant of the matrix $P - S$ to be 0. Using the parameterized equation for P leads to the following linear algebraic eigenvalue problem

$$\tilde{h}\psi = \varepsilon\psi\,, \quad \text{with} \quad \tilde{h} = C + \sqrt{\Delta}\,(S^{-1} - \gamma)^{-1}\,\sqrt{\Delta}$$

Since parameter S is determined only by the crystal structure, the sources of fluctuations here are only parameters C and Δ.

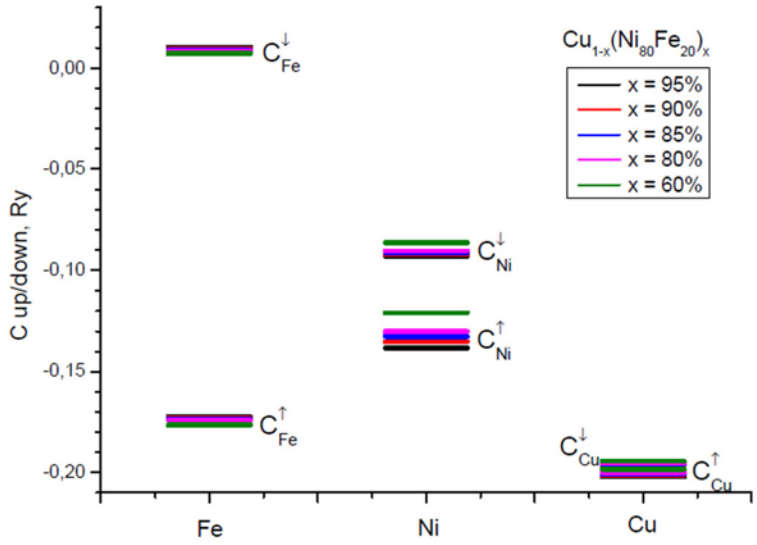

Fig. 8. The potential parameter, C, representing the d band centers of Fe, Ni, and Cu for majority (up) and minority (down) spin. Figure shows a large misalignment of the bands between alloy constituents causing strong scattering of the minority carriers at and near the Fermi level.

The band parameter C is analogous to the on-site energy in tight-binding theory and is the band center of a partial wave; Δ is the bandwidth parameter. Of particular relevance here is the parameter C for the transition metal d states. In these alloys, by far the largest determinant of alloy scattering is the mismatch in C between the alloy constituents (see **Fig. 8**). This is expected because the mismatch is large (of order 1 eV), and it is borne out in the calculations below.

In the magnetic case, C splits into one energy level for each spin, $C^{\uparrow}$ for the majority spin and $C^{\downarrow}$ for the minority spin. The average value $(C^{\uparrow} + C^{\downarrow})/2$ is approximately independent of the local magnetic moment, m, and is deeper in energy as one moves to the right across the d series. The splitting $(C^{\uparrow} + C^{\downarrow})/2$ is weakly dependent on Z, but is strongly dependent on the magnetic moment m. The Stoner parameter, I, can be defined in this theory as $I = \partial(C^{\uparrow} - C^{\downarrow})/\partial m$. For the 3d elements, I is close to 1 eV. Thus the splitting $(C^{\uparrow} - C^{\downarrow})$ can be directly related to the local moment.

Fig. 8 shows $C^{\uparrow}$ and $C^{\downarrow}$ for $Cu_{1-x}(Ni_{80}Fe_{20})_x$ alloys. Several points are evident:

- The average value on a site, $(C^{\uparrow} + C^{\downarrow})/2$ is deepest in Cu (Z = 29), higher for Ni (Z = 28), and considerably higher for Fe (Z = 26). The average value on all sites is approximately independent of x.

- The spin splitting on the Fe site ($C^{\uparrow} - C^{\downarrow}$) is robust and independent of x. This is because Fe has a strong local moment that is weakly dependent on environment.
- On the Ni site, ($C^{\uparrow} - C^{\downarrow}$) depends on the Cu concentration. The splitting is several times smaller than for Fe because the local Ni moment is smaller by a similar factor. Moreover the splitting decreases with increasing x because addition of Cu quenches the Ni moment.
- On the Cu site, ($C^{\uparrow} - C^{\downarrow}$) is very small. Cu, with its filled d shell, has almost no local moment.

As noted above, the misalignment in the value of C among alloy constituents is the primary source of scattering. Since alloy scattering is strong, other sources of scattering such as spin-orbit coupling are much weaker (which can be seen by the size of spin-orbit corrections to Hamiltonian), and to a good approximation we can consider the spin channels as almost independent. With **Fig. 8** in mind, compare the mismatch in $C^{\uparrow}$ in the series Fe-Ni-Cu. Ni is higher than both Fe and Cu. For $C^{\downarrow}$, Ni sits between Fe and Cu. There is a large mismatch for both; for this reason we expect the minority channel lifetime to be much smaller than the majority, as is borne out in the calculations.

Fig. 9a shows the change in total magnetization as a function of x and y in $Cu_yNi_{1-x-y}Fe_x$ alloys. As expected, the local magnetic moment, m, increases with x and decreases with y. The calculated results track reasonably well the experimental values, though they are somewhat larger. The discrepancy with experiment probably originates from the LDA's neglect of spin fluctuations, which causes m to be overestimated [29].

Fig. 9b shows the scattering lifetime of the minority spin near X, estimated from the width of the spectral function for a quasiparticle level crossing the Fermi level near X. See the minority spin band structure near X, Fig. 7. The lifetime decreases with either Fe or Cu concentration, as alloy scattering increases. **Fig. 9c** shows the composition-weighted sum of magnetic exchange parameter J_0, which is a measure of the cost to rotate a single spin in the system. $^2/_3\, J_0$ gives us an approximate estimate of Curie temperature T_c, from a mean field analysis; see **Figs. 9d** and **10**. This estimate for T_c scales well with experimental results (**Fig. 4**) apart from a constant scaling factor. This discrepancy between measured and calculated values is a consequence of the fact

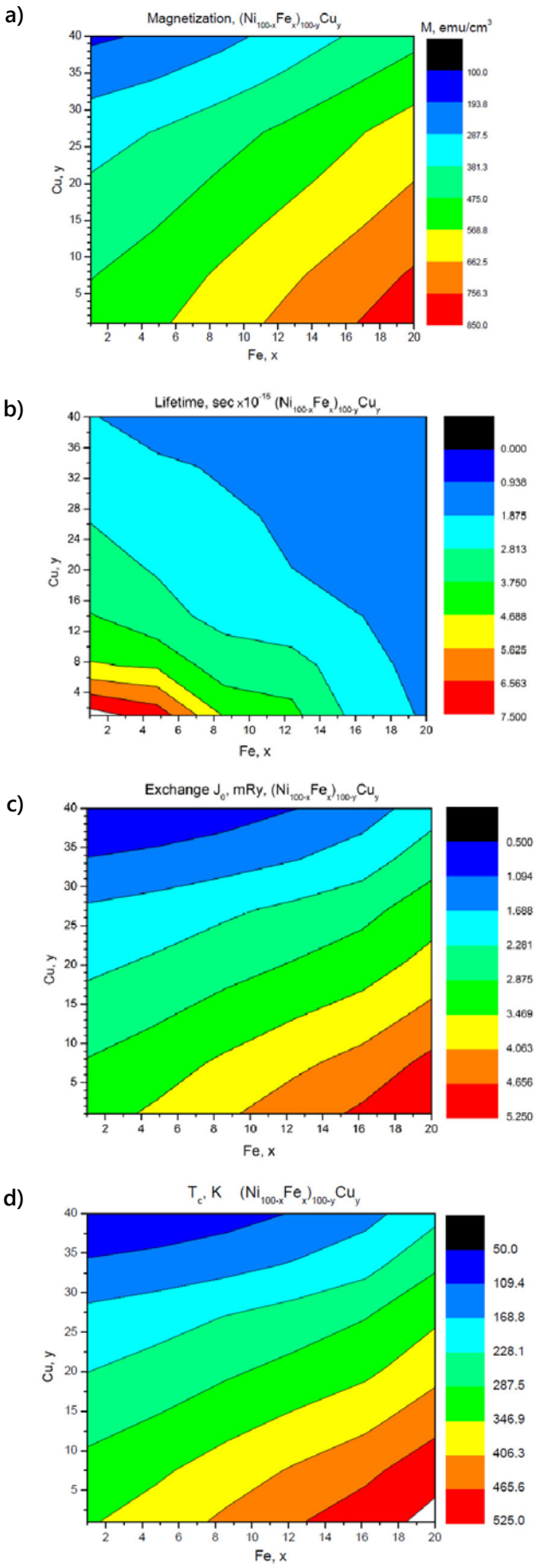

Fig. 9. Change in a) magnetization, b) lifetime, c) exchange, and d) Curie temperature T_c with the variation in the Fe (x-axis) and Cu (y-axis) content in $Cu_yNi_{1-x-y}Fe_x$. The lifetime (b) refers to the minority spin channel.

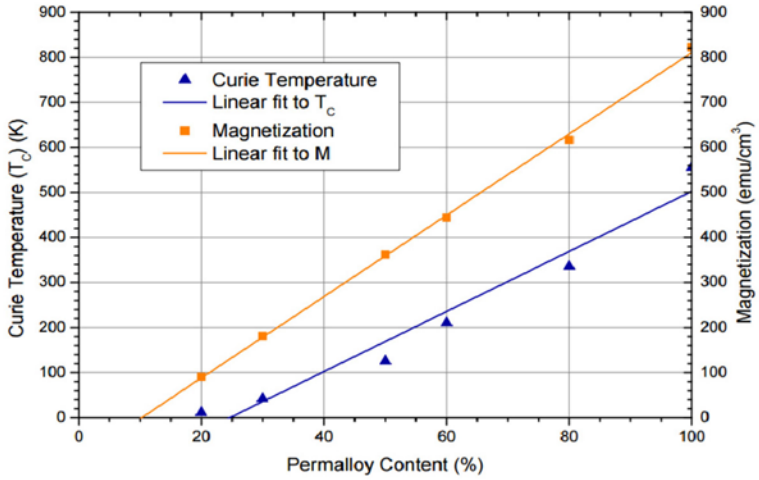

Fig. 10. Curie temperature (T_c) and magnetization (M) dependencies on Permalloy content of $Cu_{1-x}(Ni_{80}Fe_{20})_x$ obtained by CPA calculations.

that the estimate does not take into account longitudinal spin fluctuations which reduce the magnetic moment in itinerant magnets. Indeed, in elemental Ni, the average local moment approaches zero as $T \rightarrow T_c$., and only a rapidly fluctuating moment survives. **Table 2** summarizes the magnetization, lifetime and exchange parameters determined from the Local Density Approximation methods using the LMTO and CPA formalisms. It can be seen that the majority spin lifetime (calculated for a quasiparticle level crossing the Fermi level left to the X-point, see **Fig. 7**) is considerably longer than the one for the minority spin [30].

Table 2. Magnetization, lifetime and the composition-weighted sum of exchange parameters determined from the Local Density Approximation methods using the LMTO and CPA formalisms.

Alloy	M	$\tau_{up} \times 10^{-15}$, s	$\tau_{down} \times 10^{-15}$, s	J_0, mRy	J_0 (Fe)	J_0 (Ni)	J_0 (Cu)
$Ni_{99}Fe_1$	0.62	24.4	10.7	3.32	12.09	3.24	–
$Ni_{80}Fe_{20}$	1.00	23.5	1.78	5.28	11.19	3.80	–
$(Ni_{80}Fe_{20})_{80}Cu_{20}$	0.75	16.2	1.15	3.19	8.66	2.51	0.10
$(Ni_{80}Fe_{20})_{60}Cu_{40}$	0.54	13.0	0.97	2.00	6.73	1.86	0.06

5. Conclusions

To summarize, the magnetic, chemical and electrical properties of $Cu_{1-x}(Ni_{80}Fe_{20})_x$ thin films were measured. $Cu_{1-x}(Ni_{80}Fe_{20})_x$ alloys with x greater than 25% are found to be ferromagnetic. M_s and T_c of these materials are found to scale linearly with permalloy content. Alloys with x between 12% and 25% are found to have properties characteristic of superparamagnetic behavior: S-shape characteristic curves with no or small H_c, small M_r, and small squareness (M_s/M_r), and a lack of magnetic saturation even to high fields. The theoretical results show that the introduction of Cu into the permalloy lattice results in very strong spin scattering in the minority spin channel, while only moderate scattering in the majority channel. Thus, the observed much higher resistivity of copper-permalloy alloys over permalloy is from the moderately enhanced scattering of the majority spin channel. From these observations, we can conclude that $Cu_{1-x}(Ni_{80}Fe_{20})_x$ alloys appear to be attractive weak ferromagnetic materials for use in low temperature magnetoelectronic applications.

Acknowledgments — This work was supported by IARPA through Contract N66001-12-C-2020. MvS was supported by EPSRC CCP9 Flagship Project No. EP/M011631/1. RVC was supported by the ARO through grant No. W911NF-11-1-0419. The use of facilities in the LeRoy Eyring Center for Solid State Science at Arizona State University is also acknowledged.

References

[1] G. W. Elmen, Magnetic alloys of iron, nickel, and cobalt, J. The Franklin Inst. 207 (5) (1923) 538–617.

[2] R. M. Bozorth, The permalloy problem, Rev. Mod. Phys. 25 (1) (1953) 42–48.

[3] K. Binder, A. P. Young, Spin glasses: Experimental facts, theoretical concepts, and open questions, Rev. Mod. Phys. 58 (1986) 801–976.

[4] R. V. Chamberlin, D. N. Haines, Percolation model for relaxation in random systems, Phys. Rev. Lett. 17 (1990) 2197–2200.

[5] K. Szalowski, T. Balcerzak, A. Bobak, Thermodynamic properties of a dilute Heisenberg ferromagnet with interaction anisotropy – Magnetocaloric point of view, J. Mag. Magn. Mater. 323 (2011) 2095–2102.

[6] B. R. Coles, B.V.B. Sarkissian, R. H. Taylor, The role of finite magnetic clusters in Au-Fe alloys near the percolation concentration, Philos. Mag. Part B 37 (4) (1978) 489–498.

[7] D. C. Ralph, M. D. Stiles, Spin transfer torques, J. Magn. Magn. Mater. 320 (7) (2008) 1190–1216.

[8] N. D. Rizzo, M. DeHerrera, J. Janesky, B. Engel, J. Slaughter, S. Tehrani, Thermally activated magnetization reversal in submicron magnetic tunnel junctions for magnetoresistive random access memory, Appl. Phys. Lett. 80 (2002) 2335.

[9] M. A. El Qader, R. K. Singh, S. Galvin, L. Yu, J.M. Rowell, N. Newman, Switching at small magnetic fields in Josephson junctions fabricated with ferromagnetic barrier layers, Appl. Phys. Lett. 104 (2014) 022602.

[10] B. Baek, W. H. Rippard, S. P. Benz, S. E. Russek, P. D. Dresselhaus, Hybrid superconducting-magnetic memory device using competing order parameters, Nat. Commun. 5 (3888) (2014) 1–6. doi 10.1038/ncomms4888

[11] Timofei I. Larkin, Vitaly V. Bolginov, Vasily S. Stolyarov, Valery V. Ryazanov, Igor V. Vernik, Sergey K. Tolpygo, Oleg A. Mukhanov, Ferromagnetic Josephson switching device with high characteristic voltage, Appl. Phys. Lett. 100 (2012) 222601.

[12] R. Bozorth, Ferromagnetism, D. Van Nostrand Co., New York, 1951, p. 154.

[13] O. K. Andersen, O. Jepsen, Phys. Rev. Lett. 53 (1984) 2571.

[14] I. Turek, V. D. Kudrnovsky, J. Kudrnovsky, M. Sob, P. Weinberger, Electronic structure of disordered alloys, surfaces and interfaces, Kluwer, Boston, 1996.

[15] O. K. Andersen, Z. Pawlowska, O. Jepsen, Phys. Rev. B 34 (1986) 5253.

[16] H.E.H. Stremme, Phys. Lett. A 46 (2) (1973) 126–128.

[17] C. Kittel, Introduction to Solid State Physics, 7th ed., Wiley, New York, 1996, Chapt. 14.

[18] Anthony Arrott, Criterion for ferromagnetism from observations of magnetic isotherms, Phys. Rev. 108 (1957) 1394–1396.

[19] H. Kronmüller, Theory of the coercive field in amorphous ferromagnetic alloys, J. Magn. Magn. Mater. 24 (2) (1981) 159–167.

[20] C. P. Bean, J. D. Livingston, J. Appl. Phys. 30 (1959) 120.

[21] C. L. Chien, S. H. Liou, D. Kofalt, W. Yu, T. Egami, T.R. McGuire, Magnetic properties of Fe_xCu_{100-x} solid solutions, Phys. Rev. B 33 (1986) 3247–3250.

[22] R. W. Houghton, M. P. Sarachik, J. S. Kouvel, Anomalous electrical resistivity and the existence of giant magnetic moments in Ni-Cu alloys, Phys. Rev. Lett. 25 (1970) 238–239.

[23] J. Crangle, P.J.L. Butcher, Observation of resistance minima in CuNi alloys near the critical concentration for ferromagnetism, Phys. Lett. A 32 (2) (June 1970) 80–81.

[24] A. Vernes, H. Ebert, J. Banhart, Electronic conductivity in Ni_xCr_{1-x} and Ni_xCu_{1-x} fcc alloy systems, Phys. Rev. B. 68 (2003) 134404.

[25] P. E. Mijnarends, S. Sahrakorpi, M. Lindroos, A. Bansil, Phys. Rev. B 65 (2002) 075106.

[26] D. Y. Petrovykh, K. N. Altmann, H. Höchst, M. Laubscher, S. Maat, G. J. Mankey, F. J. Himpsel, Appl. Phys. Lett. 73 (1998) 3459.

[27] S. Mathias et al., Probing the timescale of the exchange interaction in a ferromagnetic alloy, Proc. Natl Acad. Sci. U.S.A. 109 (2012) 4792–4797.

[28] C. Mao-Min, N. Gharsallah, G. L. Gorman, J. Latimer, Ternary NiFeX as soft biasing film in a magnetoresistive sensor, J. Appl. Phys. 69 (1991) 5632.

[29] A. Aguayo, I. I. Mazin, D. J. Singh, Phys. Rev. Lett. 92 (2004) 147201.

[30] V. P. Antropov, M. van Schilfgaarde, S. Brink, J. L. Xu, On the calculation of exchange interactions in metals, J. Appl. Phys. 99 (2006) 08F507.